Antisense Inhibition of RNase P
MECHANISTIC ASPECTS AND APPLICATION TO LIVE BACTERIA*[S]

Heike Gruegelsiepe[‡], **Ole Brandt**[§], and **Roland K. Hartmann**[‡1]

*From the [‡]Institut für Pharmazeutische Chemie, Philipps-Universität Marburg, Marbacher Weg 6, D-35037 Marburg,
Germany and [§]Department of Functional Genome Analysis, Deutsches Krebsforschungszentrum,
Im Neuenheimer Feld 580, D-69120 Heidelberg, Germany*

We explored bacterial RNase P as a drug target using antisense oligomers against the P15 loop region of *Escherichia coli* RNase P RNA. An RNA 14-mer, or locked nucleic acid (LNA) and peptide nucleic acid (PNA) versions thereof, disrupted local secondary structure in the catalytic core, forming hybrid duplexes over their entire length. Binding of the PNA and LNA 14-mers to RNase P RNA *in vitro* was essentially irreversible and even resisted denaturing PAGE. Association rates for the RNA, LNA, and PNA 14-mers were $\sim10^5 \ M^{-1} \ s^{-1}$ with a rate advantage for PNA and were thus rather fast despite the need to disrupt local structure. Conjugates in which the PNA 14-mer was coupled to an invasive peptide via a novel monoglycine linker showed RNase P RNA-specific growth inhibition of *E. coli* cells. Cell growth could be rescued when expressing a second bacterial RNase P RNA with an unrelated sequence in the target region. We report here for the first time specific and growth-inhibitory drug targeting of RNase P in live bacteria. This is also the first example of a duplex-forming oligomer that invades a structured catalytic RNA and inactivates the RNA by (i) trapping it in a state in which the catalytic core is partially unfolded, (ii) sterically interfering with substrate binding, and (iii) perturbing the coordination of catalytically relevant Mg^{2+} ions.

Antisense-based inhibition of bacterial cell growth as a strategy to combat prokaryotic pathogens has been little-explored mainly because of the low cellular uptake efficiency of antisense agents. We report here on antisense-based inhibition of the catalytic RNA subunit of Ribonuclease P (RNase P)[2] from *Escherichia coli*. Bacterial RNase P is an essential ribonucleoprotein enzyme responsible for the 5′-end maturation of tRNAs (1) whose architecture largely differs from that of eukaryotic RNase P enzymes, a first prerequisite for a favorable drug target.

Also, its cellular abundance is low compared with ribosomal RNA or tRNA; for example, *E. coli* cells contain a 60–100-fold molar excess of ribosomes over RNase P RNA (2). Thus, compared with ribosomes, lower intracellular drug concentrations may be required to deplete cellular RNase P activity below a threshold essential for cell growth and survival. Because the enzyme contains a stable catalytic RNA subunit expected to turnover slowly relative to most mRNAs, *de novo* transcription rates of its RNA subunit are predicted to be relatively low, suggesting that its inactivation will result in a rather persistent phenotype.

Previously, the so-called P15 loop region of *E. coli*-type RNase P RNAs, known to interact with the 3′-CCA portion of precursor tRNA (ptRNA) substrates (3), was demonstrated to be a very effective target site for antisense-like inhibition strategies (4, 5). In a related but conceptually different approach termed oligonucleotide-directed misfolding of RNA, *E. coli* RNase P RNA was screened with consecutive DNA 12-mers for inhibition of ptRNA processing in a reaction mixture in which RNase P RNA was newly transcribed in the presence of its protein subunit (6). A 2′-*O*-methylated variant of one 12-mer complementary to nucleotides 289–300 in the P15 loop region turned out to be the most efficient inhibitor. This result supported our choice of the P15 loop region for the rational design of antisense agents.

Antisense strategies in general have to circumvent the problem of rapid DNA and RNA oligonucleotide degradation, and DNA additionally suffers from the relatively low stability of DNA:RNA hybrids. "Third generation" antisense agents, such as locked nucleic acid (LNA) and peptide nucleic acid (PNA), are highly resistant to degradation enzymes (7–9). In LNA, a methylene bridge connecting the 2′-oxygen and 4′-carbon atoms fixes the sugar pucker in an A-type helical conformation. PNA is composed of an uncharged peptide backbone with the nucleobases attached via methylene carbonyl linkages and is presented in a spatial arrangement mimicking natural nucleic acids. Because of its uncharged backbone, PNA was reported to be able to invade stable stem-loop structures that are not accessible to natural oligonucleotides, with helix stability being largely independent of salt concentration (10, 11). The melting temperatures of LNA:RNA duplexes are substantially increased relative to the corresponding RNA:RNA helices (12–14). The stability of LNA:RNA duplexes apparently exceeds that of PNA:RNA duplexes (15).

The most severe obstacle to inhibition of bacterial growth by antisense agents, however, is their uptake into bacterial cells. It

[2] The abbreviations used are: RNase P, Ribonuclease P; LNA, locked nucleic acid; PNA, peptide nucleic acid; ptRNA, precursor tRNA; RT, reverse transcription.

Antisense Inhibition of Bacterial RNase P

has previously been demonstrated that conjugates of PNA oligomers and invasive peptides derived from antimicrobial peptides of the innate immune system of eukaryotic organisms are able to enter Gram-negative and -positive bacteria and to interact with their specific target RNAs *in vivo* (7, 16). At present, such PNA-peptide conjugates appear to be the most efficient strategy for antisense-based inhibition of live bacteria.

Here we have characterized *in vitro* the efficiency, specificity, and kinetics of *E. coli* RNase P RNA inhibition by DNA, RNA, LNA, and PNA versions of a 14-mer complementary to the P15 loop. We further demonstrate, for the first time, the growth inhibition of live *E. coli* bacteria by an antisense oligomer specific to its highly structured and catalytic RNase P RNA. The duplex-forming oligomer inactivates the enzyme by sterically blocking substrate access, by arresting part of the catalytic core of the RNA in a non-functional conformation, and by disrupting the binding of catalytically relevant Mg^{2+} in the P15 loop region.

EXPERIMENTAL PROCEDURES

RNA, LNA, PNA, and DNA Oligonucleotides—High pressure liquid chromatography-purified RNA oligonucleotides were purchased from IBA (Göttingen, Germany) or CureVac (Tübingen, Germany). DNA oligonucleotides were from Invitrogen. Further purification of oligonucleotides was performed on denaturing polyacrylamide gels. Oligonucleotides were localized by UV shadowing, excised from the gel, eluted overnight at 8 °C in NaOAc (1 M, pH 4.9), and recovered by ethanol precipitation. The following oligonucleotides were used in this study: 5′-CAAGCA-GCCUACCC (RNA *E. coli* 14-mer), 5′-CUAGCGACCUACCC (RNA *A. vinosum* 14-mer), 5′-AAGCGGCCCAUCCC (RNA *T. thermophilus* 14-mer), 5′-CCUAUUUUUUUUACCAAAAU-UUAGG (control RNA), 5′-CAAGCAGCCTACCC (DNA *E. coli* 14-mer). The LNA 14-mer, synthesized essentially as described previously (17), was identical in sequence to the RNA *E. coli* 14-mer, except that all residues carried a locked ribose, and cytosine and uracil bases were replaced with 5-methyl-cytosine and 5-methyl-uracil. The PNA oligomers and PNA-peptide conjugates, synthesized as described previously (18), were: H_2N-caagcagcctaccc-$CONH_2$ (PNA 14-mer), H_2N-KFFKFFKFFK-G-caagcagcctaccc-$CONH_2$ (PNA-G-peptide), H_2N-KFFK-FFKFFK-AEEA-caagcagcctaccc-$CONH_2$ (PNA-AEEA-peptide), H_2N-KFFKFFKFFK-G-ccgcacactacgac-$CONH_2$ (scPNA-G-peptide; sc = scrambled), H_2N-KFFKFFKFFK-AEEA-ccgcacactacgac-$CONH_2$ (scPNA-AEEA-peptide)(AEEA = 2-aminoethoxy-2-ethoxy acetic acid linker; G = glycine).

Enzymatic RNA Synthesis, 5′-^{32}P End Labeling of ptRNA Substrate, and Kinetics—The $ptRNA^{Gly}$ substrate and RNase P RNAs were synthesized by T7 runoff transcription and purified as described previously (4, 5), and *Allochromatium vinosum* RNase P RNA from plasmid pAB12 linearized with ClaI (19). 5′-^{32}P End labeling and processing assays catalyzed by bacterial RNase P RNAs were performed as described previously (4).

3′-^{32}P End Labeling of RNase P RNA, Pb^{2+}-induced Hydrolysis, and RNase T1 and Alkaline Hydrolysis—3′-^{32}P End labeling of *E. coli* RNase P RNA, Pb^{2+}-induced hydrolysis as well as RNase T1 and alkaline hydrolysis were performed essentially as described previously (5). Radioactive bands were visualized

using a Bio-Imaging analyzer FLA 3000 –2R (Fujifilm) and the analysis software PCBAS/AIDA (Raytest). Images were further edited by Corel Photopaint, version 11.

Cloning of Bacillus subtilis rnpB in Plasmid pSP64—*B. subtilis rnp*B, including its natural promoter and terminator, was amplified from genomic *B. subtilis* DNA (strain W168) using primers 5′-GGC AGC AAG CTT TAT GAT TGA TCA C (including the native HindIII site upstream of *rnp*B) and 5′-CGC CCA AGC TTG TGT ATA CTT CTT CAT CGT ATC ACC CTG TC. The resulting PCR fragment was cloned in the HindIII site of pSP64 (Promega).

E. coli Growth Inhibition Experiments—PNA-peptide conjugates were tested for inhibition of *E. coli* cells (wild-type K12 and the lipopolysaccharide-defective *E. coli* strain AS19; Ref. 20) essentially as described in Ref. 7. 3 ml of LB (Luria-Bertani) medium were inoculated with a single colony, and cells were grown under aeration (180 revolutions/min in a thermoshaker) at 37 °C to an A_{578} of 2.4 –3.7. Suspensions were diluted with double-distilled H_2O (strain K12) or 0.9% NaCl (strain AS19) to 10% LB and 5×10^5 cells/ml. To 100 μl (5×10^4 cells) of such a suspension, PNA-peptide inhibitor was added and 10 μl aliquots withdrawn after 0, 10, 30, 60, and 180 min; aliquots or appropriate dilutions (down to 1:10,000) were plated in 10 (for undiluted samples) or 100 μl portions (in 10% LB, including 0.9% NaCl for strain AS19), incubated on LB agar plates at 37 °C overnight, and the number of colonies counted.

Reverse Transcription (RT)-PCR—To compare *E. coli* RNase P RNA levels in inhibited and uninhibited cells, AS19 cells harboring plasmid pSP64-*Bsrnp* were grown as described above and treated with either no inhibitor, 5 μM PNA-G-peptide, or 5 μM scPNA-G-peptide for 3 h. Cell amounts were verified by plating. Total RNA from each culture was prepared using the RNeasy Mini Kit (Qiagen) followed by DNase I treatment (Promega). RT-PCR was performed with the AccessQuick RT-PCR System (Promega) according to the manufacturer's instructions. Primers specific for *E. coli rnpB* were 5′-CTC ACT GGC TCA AGC AGC CT (5′-end-labeled) and 5′-GAA GCT GAC CAG ACA GTC GC. Primers specific for *rpsR* (ribosomal protein S18) were 5′-TGG CAC GTT ATT TCC GTC G (5′-end-labeled) and 5′-TTA CTG ATG GCG ATC AGT GTA CGG. RT-PCR reactions contained the normal amounts of unlabeled primers and, in addition, trace amounts of the respective 5′-end-labeled primer.

RESULTS

Inhibition Efficiency and Specificity of DNA, RNA, LNA, and PNA 14-mer Versions—Hybrid formation of the 14-mer (*E. coli* 14-mer; either RNA or DNA) with its target site in the P15 loop region of *E. coli* RNase P RNA (Fig. 1) results in the disruption of the local structure and blocks the docking of the tRNA 3′-end to the active site of RNase P RNA (5). This inhibits RNase P activity, not only in the RNA alone but also in the holoenzyme reaction (4). We extended our inhibition analyses by including derivatives of the 14-mer containing a PNA or LNA backbone. As a first approach to assessing the relative binding affinities of the RNA, DNA, LNA, and PNA oligomer versions, we preincubated *E. coli* RNase P RNA with different oligomer concentrations for ≥40 min to allow the binding equilibrium to be

reached. Multiple turnover processing reactions containing 10 nM RNase P RNA were then started by adding 100 nM ptRNA substrate. Inhibition efficiencies (given as K_i values, defined as the oligomer concentration resulting in a 2-fold reduced rate of ptRNA cleavage) (Table 1) provided a first measure for the relative inhibitor strength. K_i values do not necessarily equal K_D values but report the same trends in binding affinity differences (5). The RNA and LNA variants turned out to have the lowest

FIGURE 1. **Secondary structure of *E. coli* RNase P RNA.** The target region of the 14-mer (nucleotides 291–304) is indicated by the *bold line*. *P*, helical regions; *J*, joining segments named according to the helices they connect. The two guanosines (G292 and G293) that form Watson-Crick base pairs with C74 and C75 of tRNA 3′-ends are *highlighted* and *boxed*. Prominent lead cleavage sites are marked by *roman numerals*.

and very similar K_i values (2.2 for RNA, 3.9 for LNA) (Table 1) followed by PNA ($K_i = 12.5$) and DNA ($K_i = 25$). K_i values of 2–4 nM are low for an enzyme concentration of 10 nM, as one would expect 5 nM to be the minimum inhibitor concentration for obtaining 50% inhibition. We attribute this to the finding that only ~50–60% of *E. coli* RNase P RNA is in an active conformation after 40 min of preincubation at 37 °C in the standard buffer used here (21).

We then addressed the inhibition specificity of the RNA, LNA, and PNA versions of the 14-mer by testing their effects on the processing reaction catalyzed by three other bacterial RNase P RNAs with sequence variation in the target region, namely those from *Pseudomonas aeruginosa*, *A. vinosum*, and *Thermus thermophilus*. Complementarity of the *E. coli* 14-mer was predicted to be the least compromised with *P. aeruginosa* RNase P RNA, of intermediate stability for the *A. vinosum* RNA, and most destabilized for *T. thermophilus* RNase P RNA (Fig. 2). As expected, inhibition efficiencies of RNA and PNA 14-mers decreased in the order *P. aeruginosa* > *A. vinosum* > *T. thermophilus* (Table 1). Yet with the LNA 14-mer, there was little discrimination. This is attributable to the extraordinary stability of LNA:RNA hybrids (12, 13), which leads to increased mismatch tolerance, in line with a previous study (15).

In a reverse setup, we designed 14-meric RNA oligomers that fully matched the P15 loop region of *A. vinosum* and *T. thermophilus* RNase P RNA, respectively. For the *A. vinosum* 14-mer, the 53-fold discrimination against *E. coli* RNase P RNA ($K_i = 3.0$ *versus* 160) (Table 1) exactly mirror-imaged what we had seen with the *E. coli* 14-mer (Table 1). Surprisingly, discrimination against the *E. coli* RNase P RNA was only 6-fold for the *T. thermophilus* 14-mer (for details, see supplemental Fig. S1).

Invasion of PNA and LNA 14-mers into the P15 Loop Region— We next analyzed strand invasion of the 14-mers into the P15 loop region of *E. coli* RNase P RNA by lead probing. For the RNA and DNA 14-mers, we had shown earlier (5) that they anneal to the target region over their entire length, as inferred from the suppression of lead hydrolysis in the region spanning nucleotides 291–304 of RNase P RNA (Fig. 3, *lanes 11* and *12*). In addition, a novel lead hydrolysis product appears in the 5′-proximal strand of helix P15 (Fig. 3, *arrow*), demonstrating that P15 is disrupted in oligomer-RNase P RNA complexes. The *T. thermophilus*-specific RNA 14-mer induced the same changes under the conditions applied (Fig. 3, *lanes 9* and *10*). Incomplete suppression of lead cleavage at site V is attributable
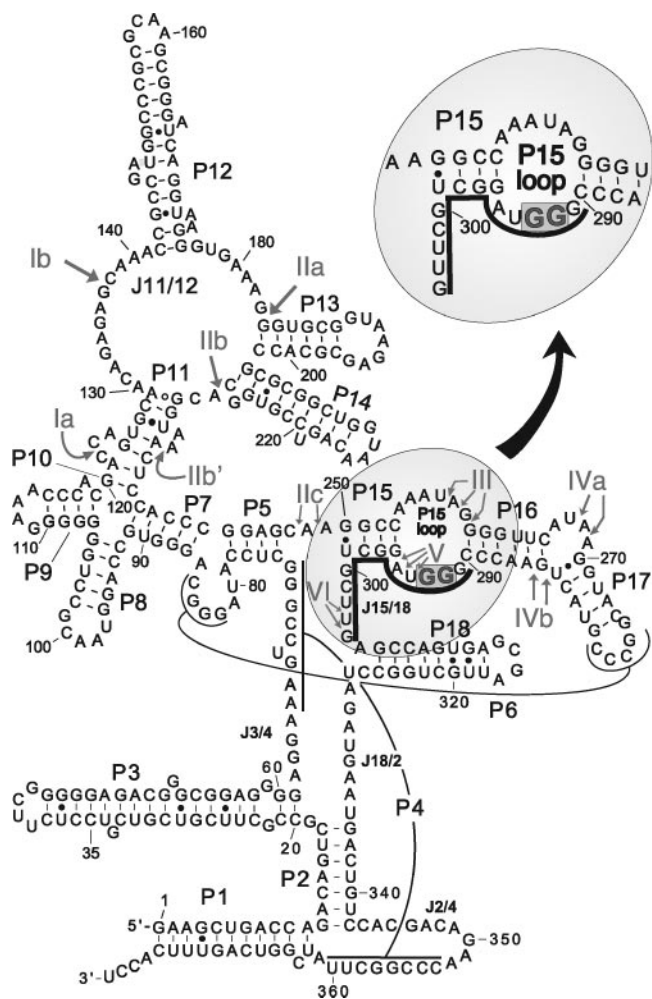
TABLE 1

K_i and k_{on} values for the binding of antisense 14-mers to RNase P RNAs

14-mers were preincubated with RNase P RNAs for 40 min (80 min for the LNA 14-mer); at 37 °C in buffer I (0.1 M NH₄ OAc, 0.1 M Mg(OAc)₂, 50 mM Hepes, pH 7.0). Mean K_i values are based on at least three independent experiments; NA, not analyzed. In the first column, deviations from perfect Watson-Crick complementarity are indicated in parentheses for interaction of the *E. coli* 14-mer with the heterologous RNase P RNAs; GU, G-U wobble pair; k_{on} values (in M⁻¹ s⁻¹) are given in bold below K_i values for *E. coli* RNase P RNA.

| RNase P RNA	*E. coli* 14-mer, RNA, K_i	*E. coli* 14-mer, LNA, K_i	*E. coli* 14-mer, PNA, K_i	*E. coli* 14-mer, DNA, K_i	*A. vinosum* 14-mer, RNA, K_i	*T. thermophilus* 14-mer, RNA, K_i
			K_i *values in nM*			
E. coli	2.2 ± 0.6	3.9 ± 1.8	12.5 ± 0.5	25 ± 5	160 ± 10	80 ± 20
k_{on}	$(6.8 ± 0.7) × 10^4$	$(8.6 ± 4.5) × 10^4$	$(2.2 ± 0.5) × 10^5$	$(2.3 ± 2.0) × 10^4$		
P. aeruginosa (1 mismatch, 1 GU)	19.0 ± 1.5	18.2 ± 0.8	580 ± 225	NA	NA	NA
A. vinosum (2 mismatches, 1 GU)	125 ± 53	25 ± 5	3200 ± 1500	NA	3.0 ± 0.6	NA
T. thermophilus (1 mismatch, 1 GU, 1 bulge)	1200 ± 25	36 ± 13	7000 ± 3000	NA	NA	13.3 ± 2.5
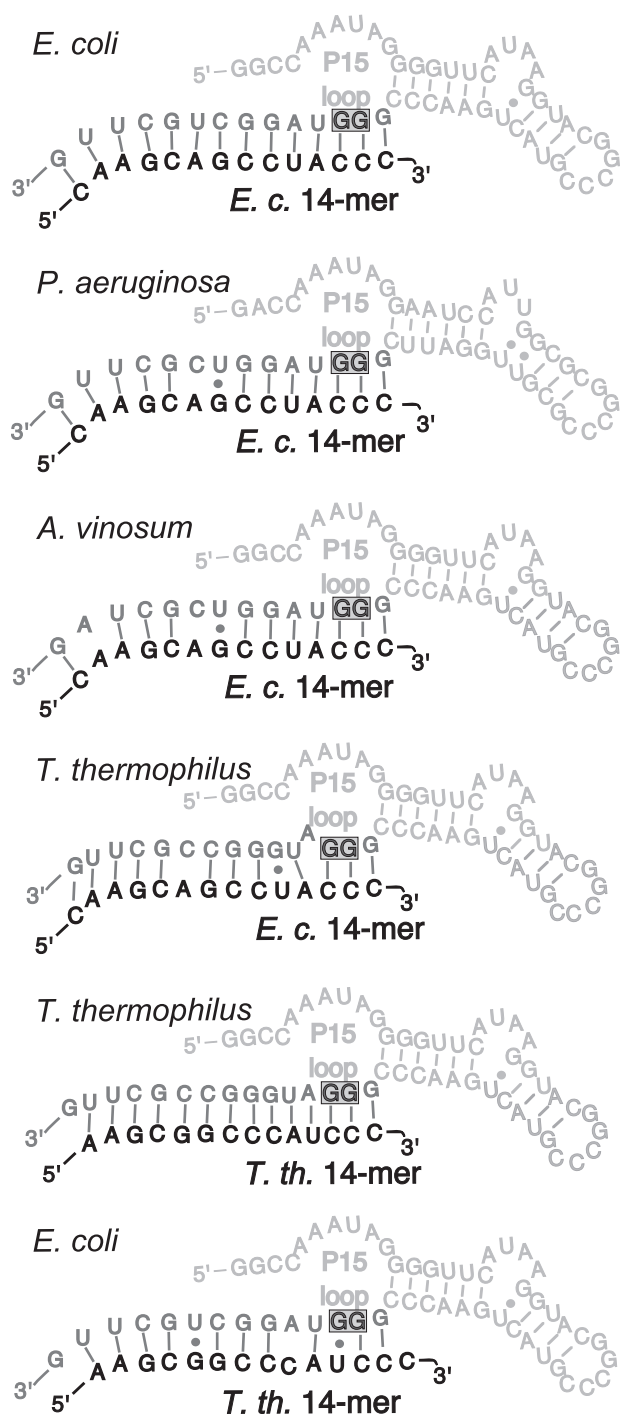
FIGURE 2. **Expected duplexes formed between the *E. coli*-specific 14-mer (*E. c.* 14-mer) and bacterial RNase P RNAs from *E. coli*, *P. aeruginosa*, *A. vinosum*, and *T. thermophilus*.** Duplex formations between the 14-mer specific to *T. thermophilus* RNase P RNA (*T. th.* 14-mer) and its cognate or *E. coli* RNase P RNA are depicted in the two sketches at the *bottom*. Individual P15 loop regions are shown in *gray letters*, and the two guanosines corresponding to G292 and G293 of *E. coli* RNase P RNA are *highlighted* in *boxes*. For more details, see Fig. 1.

FIGURE 3. **Pb²⁺-induced hydrolysis pattern.** Shown are the Pb²⁺ hydrolysis patterns of 3′-³²P-labeled *E. coli* RNase P RNA (10 nM) in the presence of either 500 nM RNA, LNA, or PNA *E. coli* 14-mer (*lanes 11–16*) or 6.5 μM *T. thermophilus* 14-mer (*lanes 9* and *10*) or of an unrelated control RNA 25-mer at 6.5 μM (*lanes 7* and *8*). *Lanes 1* and *2*, limited hydrolysis of *E. coli* RNase P RNA by RNase T1 under denaturing conditions or by alkaline hydrolysis (*A*); *lanes 3* and *4*, radio-labeled *E. coli* RNase P RNA either directly loaded onto the 15% PAA/8 M urea gel (*C1*) or incubated in hydrolysis buffer (0.1 M Mg(OAc)₂, 0.1 M NH₄OAc, 50 mM Tris-HCl, pH 7.1) without lead acetate for 50 min at 37 °C (*C2*). *Left margin*, assignment of G-specific RNase T1 fragments according to the numbering system for *E. coli* RNase P RNA (see Fig. 1); *right margin*, corresponding assignment of Pb²⁺-hydrolysis bands; *dotted line*, area protected by the 14-mers; *horizontal arrow*, new hydrolysis product that appears upon disruption of helix P15. The lead cleavage pattern, although remaining essentially identical, is upshifted in *lanes 13–16*, because LNA and PNA 14-mers stick to RNase P RNA fragments containing the target region, even under denaturing gel conditions.

to imperfect complementarity and thus decreased affinity of this oligomer for *E. coli* RNase P RNA (Fig. 2). The lead cleavage pattern remained unchanged upon the addition of a control RNA lacking substantial sequence complementarity to *E. coli* RNase P RNA (Fig. 3, *lanes 7* and *8*). In the presence of the *E. coli*-specific LNA 14-mer (*lanes 13* and *14*), the same changes
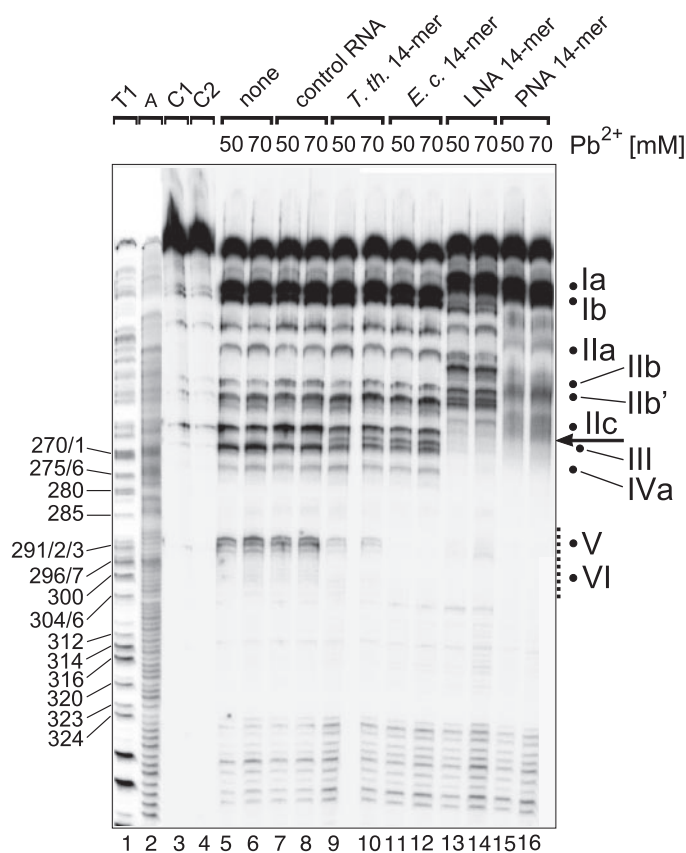
in the lead cleavage pattern as for the RNA analog were seen. However, all fragments that included the target site were shifted toward lower gel mobility, whereas the smaller ones (Fig. 3, *bottom section* of the gel) excluding this region showed unperturbed mobility. This result demonstrates that the LNA 14-mer remained bound to the RNase P RNA, even during electrophoresis in the presence of 8 M urea. A very similar observation was made with the PNA 14-mer (Fig. 3, *lanes 15* and *16*), but there the upshifted fragments migrated more diffusely. One explanation is that the PNA 14-mer undergoes dissociation and reassociation cycles during electrophoresis. Alternatively, PNA is known to have a propensity to form RNA:PNA₂ triplexes (22). Triplex formation is indeed conceivable based on the sequence of the PNA 14-mer (supplemental Fig. S2) and might have contributed to the diffuse gel mobility in *lanes 15* and *16* (Fig. 3).

Inhibitor Association Rates—The lead probing experiments (Fig. 3) indicated that hybrid helices formed between the LNA
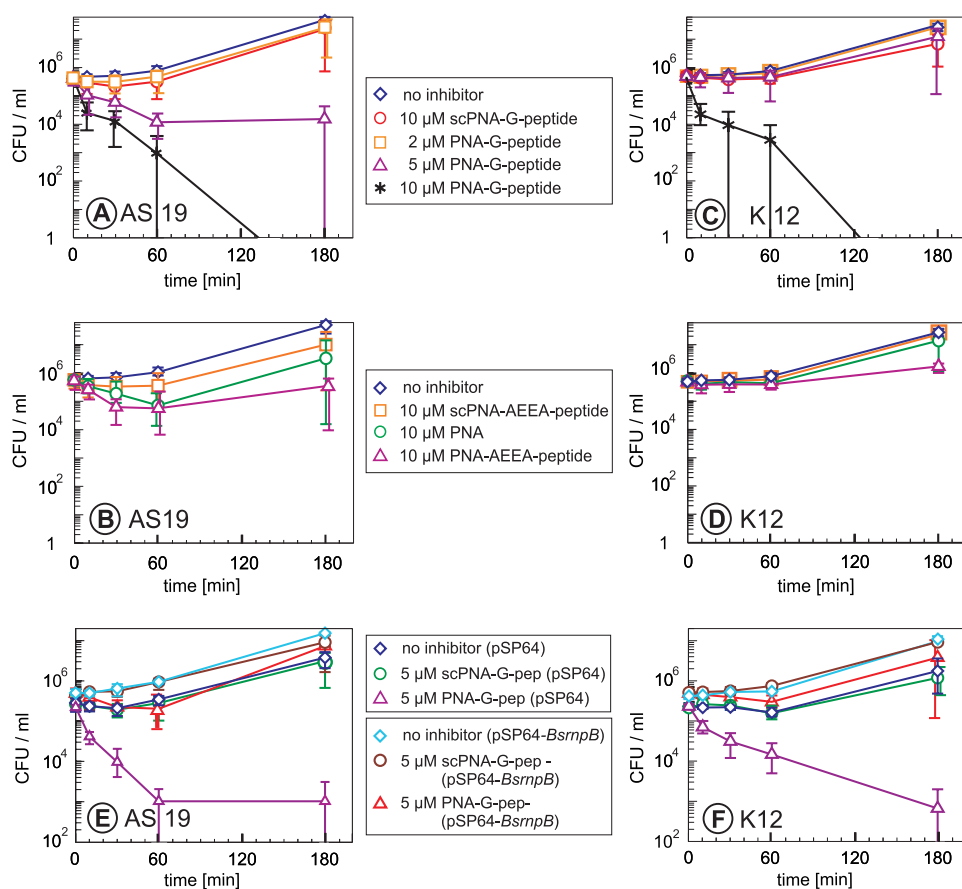
FIGURE 4. **Analysis of growth inhibition of *E. coli* AS19 (*A* and *B*) and K12 (*C* and *D*) cells by *E. coli* RNase P RNA-specific PNA inhibitors and rescue of growth inhibition by the PNA-G-peptide upon expression of plasmid-encoded *B. subtilis* RNase P RNA (*E* and *F*).** Cell suspensions (in 10% LB broth) were incubated with PNA and PNA-peptide conjugates (type and concentration indicated in the *center boxes*) for different time periods followed by a plating assay to count the number of colony-forming cells (see "Experimental Procedures"). With 10 μM PNA-G-peptide, not a single colony survived after 180 min (*A* and *C*), which explains why the curves hit the *x*-axis in these cases; *sc*, scrambled control PNA-peptide conjugate with a PNA moiety of a different sequence but identical nucleobase composition; pSP64, empty cloning plasmid; pSP64-*BsrnpB*, pSP64 derivative carrying the *B. subtilis* RNase P RNA gene (*rnpB*) under control of its native promoter (for plasmid construction, see "Experimental Procedures"). Data points represent mean values of 3– 8 individual experiments with error ranges indicated by *error bars*; the *lower* part of the error bars was the highest in experiments with the most potent PNA-G-peptide, where cell survival was on the borderline. Here we had a subset of individual experiments with very low colony-forming units (*CFU*)/ml values (down to zero in some cases) and another with substantially higher CF units/ml values.

or PNA 14-mer and the target region dissociate at very slow rates (k_{off}). Because the RNA 14-mer was previously shown to dissociate at a rate not exceeding 0.02 h^{-1} under processing assay conditions (5), k_{off} could be considered as practically zero for the RNA, LNA, and PNA 14-mers within the time frame of our inhibition analyses. We then addressed the question as to which extent these analogs may differ from their natural DNA and RNA counterparts in the rate of association (k_{on}). This was analyzed by an RNase P RNA activity assay performed under conditions where processing activity linearly depended on the amount of active enzyme. Thus, we determined the fraction of active (uninhibited) enzyme that remained after increasing enzyme-oligomer preincubation times, and the rate of enzyme inactivation equaled the rate of oligomer association (for details, see supplemental Fig. S3). The PNA 14-mer showed the fastest rate followed by the LNA and RNA versions and the DNA 14-mer with the slowest association rate (Table 1, values in bold lettering).

Inhibition by PNA-Peptide Conjugates in Vitro—Limited cellular uptake is a general problem of antisense agents, especially in bacteria. Because improved cell entry was demonstrated for PNA oligomers coupled to invasive peptides (7), we adopted this strategy for RNase P inhibition. Taking into account that the linker connecting the N-terminal peptide and the PNA oligomer may influence inhibition efficacy (7, 23), we utilized two different linkers. One is the commonly used 2-amino-ethoxy-2-ethoxy acetic acid (AEEA) linker, (also termed 8-amino-3,6-di-oxaoctanoic acid linker and abbreviated as eg1) (7, 24); and the other is the novel shorter monoglycine linker not analyzed so far (supplemental Fig. S4*A*). We first tested these PNA-peptide conjugates in our standard RNA-alone processing assay (see Table 1). At a concentration of 100 nM, both the PNA-AEEA-peptide and PNA-G-peptide completely inhibited processing, in contrast to a control AEEA conjugate containing a scrambled PNA 14-mer (supplemental Fig. S4*B*). Similar results were obtained in the *E. coli* RNase P holoenzyme assay (supplemental Fig. S4*C*). There, specific inhibition was already evident at the lower concentration (12.5 nM) of PNA 14-mer or PNA-G-peptide.

Inhibition by PNA-Peptide Conjugates in Vivo—The conjugates were then tested for *in vivo* inhibition of *E. coli* wild-type K12 and a more permeable mutant strain (AS19) defective in lipopolysaccharide synthesis (20). To this end, cell suspensions were incubated with the corresponding conjugate for up to 180 min followed by a plating assay to determine the number of surviving colony-forming cells. Incubation of AS19 cells at 10 μM PNA-G-peptide for 180 min did not leave any survivors in all experiments, whereas inhibition by 5 μM was, on average, substantial but incomplete (Fig. 4*A*). Surprisingly, inhibitor effects were less pronounced with the PNA-AEEA-peptide (Fig. 4*B*) containing the linker used in a related previous study (7). 10 μM PNA-AEEA-peptide had a much weaker inhibitory effect than the PNA-G-peptide at the same concentration. Scrambled versions of the two conjugate types showed a very mild inhibitory effect, suggesting that 10 μM is at the threshold of concentrations at which PNA-peptide conjugates start to inhibit *E. coli* cells in an antisense-independent manner. The minimal inhibitory concentration of the decamerpeptide (KFF)$_3$K itself was reported as 30 μg/ml (~20 μM) for *E. coli* K12 strains (25). Thus, the carrier peptide moiety may well be

the cause of the weak nonspecific inhibition effects seen here. Inhibition effects were not markedly different for the K12 compared with the AS19 strain but somewhat attenuated (Fig. 4*C*). This is consistent with the more permeable cell barrier of the AS19 mutant strain. The PNA 14-mer alone also showed some inhibition at a concentration of 10 μM (more pronounced with the AS19 relative to the K12 strain) (Fig. 4, *B* and *D*).

To demonstrate intracellular PNA-peptide association with RNase P RNA, we performed a genetic complementation experiment. The *B. subtilis* RNase P RNA gene (*rnpB*) was previously shown to be able to functionally replace the native *E. coli rnpB* gene *in vivo* (26, 27). We also did not observe inhibition of *B. subtilis* RNase P RNA by oligonucleotides targeted to the P15 loop region of *E. coli* RNase P RNA (4). AS19 and K12 bacteria transformed with a plasmid expressing *B. subtilis rnpB* (pSP64-*BsrnpB*) indeed rescued inhibition caused by the presence of the PNA-G-peptide (Fig. 4, *E* and *F*), further supporting the specificity of inhibition. Transformation with the multicopy plasmid pSP64 and growth in the presence of the antibiotic ampicillin made the AS19 and K12 bacteria somewhat more sensitive to inhibitors, which explains why we observed a more pronounced inhibition effect at 5 μM PNA-G-peptide compared with the data in Fig. 4, *A* and *C*.

In addition, RT-PCR was applied to analyze the fate of *E. coli* RNase P RNA upon inhibition by the PNA-G-peptide. AS19 bacteria harboring the complementation plasmid pSP64-*BsrnpB* were used, which had the advantage that cell growth was nearly the same in the presence and absence of PNA-G-peptide due to the expression of *B. subtilis* RNase P RNA (Fig. 4, *E* and *F*). The mRNA encoding ribosomal protein S18 (*rpsR*) was used to control for fluctuations in RNA template amounts used for RT-PCR reactions. Levels of *E. coli* RNase P RNA were clearly decreased in cells incubated with the PNA-G-peptide but not in those treated with the scrambled control conjugate (Fig. 5), suggesting that complexation with the inhibitor induces RNase P RNA degradation.

DISCUSSION

Our starting point was an RNA 14-mer that had the strongest inhibition effect on *in vitro* processing by *E. coli* RNase P RNA among several related oligoribonucleotides (5). To study stabilizing oligomer modifications in a systematic manner and for comparability reasons, we analyzed the PNA and LNA versions of the identical sequence and (in the case of the LNA 14-mer) carrying this ribose modification at each nucleotide position. We were aware that oligonucleotides with LNA modifications at only a few positions might be preferable for antisense strategies, as the gain in duplex stabilization ($\Delta T_m/°C$) per LNA modification is maximal if only, for example, every third nucleoside is replaced with the analog (12). Our *in vitro* inhibition experiments have shown that the RNA, DNA, PNA, and LNA versions of the 14-mer disrupt the structured P15 loop region of type A RNase P RNAs, forming a hybrid duplex over the entire oligomer length (Fig. 3) (5). Beyond disruption of the catalytic core structure, oligomer invasion prevents anchoring of tRNA 3′-NCCA-ends to the P15 loop and, thereby, perturbs coordination of catalytically relevant Mg^{2+} (28). The rate of dissociation was negligible for RNA, LNA, and PNA 14-mers under the
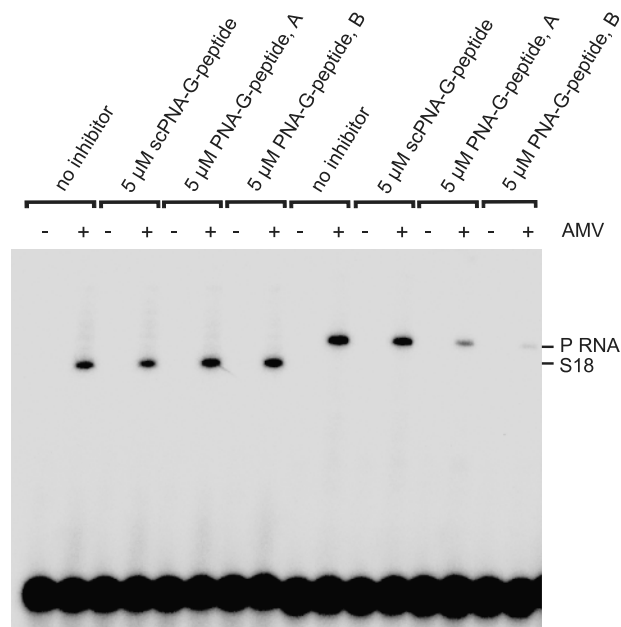

FIGURE 5. **RT-PCR to analyze the cellular level of *E. coli* RNase P RNA upon treatment with the PNA-G-peptide.** Total RNA was isolated from AS19 bacteria expressing *B. subtilis* RNase P RNA from plasmid pSP64-*BsrnpB* as in Fig. 4*E*. *AMV*, reverse transcriptase; *sc*: scrambled control PNA-peptide conjugate with a PNA moiety of a different sequence but identical nucleobase composition. *A* and *B* indicate two different samples. The reduction in the amount of RT-PCR product corresponding to *E. coli* RNase P RNA from cells treated with the PNA-G-peptide was seen in five independent experiments, with the ratio of radioactivity for the product specific for *E. coli* RNase P RNA *versus* S18 mRNA decreasing by a factor of $\geq$4.

applied conditions. The extraordinary stability of the target RNA-LNA duplex was associated with reduced discrimination against mismatched target sequences (Table 1) consistent with previous observations (15). The PNA 14-mer combined excellent specificity and the fastest association rate among the inhibitors tested (Table 1). Its relatively high K_i value (12.5 nM) (Table 1) can be explained by a certain propensity of hydrophobic PNA to self-aggregate (29), which likely reduced the effective concentration of PNA single strands, although we tried to minimize this problem by preparing, handling, and quantifying PNA solutions at 80 °C. At explicitly smaller oligomer sizes, however, LNA may become advantageous over PNA. For example, an LNA 8-mer directed against the telomerase RNA subunit inhibited telomerase in human prostate cancer cells with an IC_{50} of 25 nM, whereas a corresponding PNA 8-mer had a 200-fold lower potency; an LNA 8-mer with a single mismatch showed an at least 40-fold lower efficacy (15). One may argue that LNA octamers might elicit substantial off-target effects because of the multiple occurrence of identical octanucleotide sequences in bacterial and eukaryotic genomes. However, it is rather unlikely that oligomer annealing to sequence-identical non-target sites, if accessible to hybridization at all, entails the similarly severe functional consequences as duplex formation with the specific target site. Indeed, transfection of a human cell line with the aforementioned telomerase RNA subunit-specific LNA 8-mer did not reveal any signs of toxicity (15). These results, although not conclusive yet, are encouraging in the exploration of whether LNA-modified oligomers of <10 nucleotides may substantially

improve entry into bacteria without a substantial decrease in target selectivity or increase in toxicity.

Measured association rates (k_{on}) for the RNA, LNA, and PNA 14-mers were in the range of 10^5 M^{-1} s^{-1} (Table 1). The value for the RNA 14-mer was previously calculated to be close to 10^4 M^{-1} s^{-1} based on experimentally determined values for k_{off} and K_D (5). We consider the direct experimental determination of k_{on} reported here to provide the more accurate values. The value of 10^5 M^{-1} s^{-1} is only a factor of ~10 below the values observed for natural antisense systems and exceeds the association rates of many artificial antisense interactions by a similar factor (30, 31). We conclude that the oligomer annealing to the P15 loop region is rather fast despite the need to disrupt the helix P15 and possibly additional tertiary interaction in the catalytic core of RNase P RNA. This finding may be related to the fact that the P15 loop has been optimized during evolution as a binding site for the single-stranded 3′-overhangs of tRNA molecules. Mechanistically, oligomers may initially interact with the fully accessible CCA-binding loop and, during transient thermal opening of helix P15, snap into the P15 target sequence to extend base pairing in a zipper-like manner. When base pairing is established over the entire oligomer length, the RNase P RNA is trapped in the partially unfolded conformation, which appears to trigger RNA degradation *in vivo* (Fig. 5). Based on our results, it should be worthwhile to explore the loop of helix 80 of 23 S rRNA by a very similar antisense strategy, as G2251 and G2252 in this loop form Watson-Crick pairs with C74 and C75 of tRNA bound to the P site (32).

The PNA oligomer was coupled to an artificial carrier peptide that was shown to facilitate bacterial uptake in a previous study (7). Here, we could further improve efficacy of such conjugates by introducing a novel monoglycine linker connecting PNA and the carrier peptide. The monoglycine linker seems to improve bacterial uptake, as conjugates with the monoglycine and AEEA linker inhibited processing by RNase P RNA *in vitro* to very similar extents (supplemental Fig. S4). Invasive peptides of the type used here, rich in basic and hydrophobic residues, form amphipathic secondary structures and interact preferentially with bacterial membranes whose outer layers expose anionic groups for electrostatic interactions; the presence of cholesterol in eukaryotic membranes contributes to the preference of these peptides for bacterial membranes (33). The preference of invasive peptides for bacterial membranes may reduce (but not necessarily eliminate) their potential toxicity in therapeutic applications. Indeed, the (KFF)$_3$K-type peptides are able to induce histamine release in some mammals (16) and hemolysis of human erythrocytes (25). Several other peptides were recently coupled to PNA antisense oligomers and tested for target inhibition in live *Staphylococcus aureus* cells. Hexa- to decapeptides chemically unrelated to (KFF)$_3$K were found to be efficient mediators of cell entry as well (16). The use of non-cationic carrier peptides could also alleviate the problem of aggregation and precipitation of conjugates consisting of anionic oligonucleotides and cationic peptides (34). Another perspective is the synthesis of disulfide-linked oligomer-peptide conjugates that are cleaved in the more reductive milieu of the bacterial cell to release the antisense oligomer. In summary, the development of carrier peptides with optimal performance in terms of bacterial uptake efficiency, delivery to the target, pref-

erence for bacterial membranes, and low toxicity in the host will be in the focus of future studies.

In a related study, a PNA-peptide conjugate directed against the essential *fmhB* gene suppressed growth of *S. aureus* at 10 μM (16), similar to what we have observed. This inhibitor concentration was about 13 times higher than the IC$_{50}$ values for PNA-peptide-based inhibition of the non-essential *gfp* gene (16). A major reason for such discrepancies could be that IC$_{50}$ values for the inhibition of a non-essential enzyme are different from concentrations required to fully suppress bacterial growth. Complete suppression of bacterial growth is expected to only be reached when the intracellular activity level of an essential gene product is depleted far below 50% of its normal level.

PNA-based inhibition of stable RNAs has been explored to some extent for ribosomal RNA as the target (35). Two triplex-forming 7- or 12-mer PNA strands connected by an AEEA linker were tested, one directed against a single-stranded heptanucleotide sequence in the α-sarcin loop and the second against a dodecameric sequence in the peptidyl transferase center of *E. coli* 23 S RNA. In the latter case and similar to the RNase P situation reported here, triplex formation required some disruption of local 23 S rRNA structure; the IC$_{50}$ value for inhibition of AS19 cells in 0.1× LB broth was reported as 5 μM (35). With respect to the triplex-forming PNA conjugate directed against the α-sarcin loop, attachment of the (KFF)$_3$K carrier peptide improved the inhibitory effect on the growth of *E. coli* K12 cells by a factor of seven (7). These findings, combined with those presented here, are encouraging in the further progression toward the development of stable RNA-specific drugs that exploit the hydrogen bonding capacities of nucleobases.

REFERENCES

1. Frank, D. N., and Pace, N. R. (1998) *Annu. Rev. Biochem.* **67,** 153–180
2. Dong, H., Kirsebom, L. A., and Nilsson, L. (1996) *J. Mol. Biol.* **261,** 303–308
3. Kirsebom, L. A., and Svärd, S. G. (1994) *EMBO J.* **13,** 4870–4876
4. Willkomm, D. K., Gruegelsiepe, H., Goudinakis, O., Kretschmer-Kazemi Far, R., Bald, R., Erdmann, V. A., and Hartmann, R. K. (2003) *Chembiochem* **4,** 1041–1048
5. Gruegelsiepe, H., Willkomm, D. K., Goudinakis, O., and Hartmann, R. K. (2003) *Chembiochem* **4,** 1049–1056
6. Childs, J. L., Poole, A. W., and Turner, D. H. (2003) *RNA* **9,** 1437–1445
7. Good, L., Awasthi, S. K., Dryselius, R., Larsson, O., and Nielsen, P. E. (2001) *Nat. Biotechnol.* **19,** 360–364
8. Kurreck, J. (2003) *Eur. J. Biochem.* **270,** 1628–1644
9. Wahlestedt, C., Salmi, P., Good, L., Kela, J., Johnsson, T., Hökfelt, T., Broberger, C., Porreca, F., Lai, J., Ren, K., Ossipov, M., Koshkin, A., Jakobsen, N., Skouv, J., Oerum, H., Jacobsen, M. H., and Wengel, J. (2000) *Proc. Natl. Acad. Sci. U. S. A.* **97,** 5633–5638
10. Egholm, M., Buchardt, O., Christensen, L., Behrens, C., Freier, S. M., Driver, D. A., Berg, R. H., Kim, S. K., Norden, B., and Nielsen, P. E. (1993) *Nature* **365,** 566–568
11. Tomac, S., Sarkar, M., Ratilainen, R., Wittung, P., Nielsen, P. E., Nordén, B., and Gräslund, A. (1996) *J. Am. Chem. Soc.* **118,** 5544–5552
12. Singh, S. K., and Wengel, J. (1998) *Chem. Commun.* **12,** 1247–1248

13. Childs, J. L., Disney, M. D., and Turner, D. H. (2002) *Proc. Natl. Acad. Sci. U. S. A.* **99,** 11091–11096

14. Nielsen, K. E., Rasmussen, J., Kumar, R., Wesper, J., Jacobsen, J. P., and Petersen, M. (2004) *Bioconjugate Chem.* **15,** 449–457

15. Elayadi, A. N., Braasch, D. A., and Corey, D. R. (2002) *Biochemistry* **41,** 9973–9981

16. Nekhotiaeva, N., Awasthi, S. K., Nielsen, P. E., and Good, L. (2004) *Mol. Ther.* **10,** 652–659

17. Schmidt, K. S., Borkowski, S., Kurreck, J., Stephens, A. W., Bald, R., Hecht, M., Friebe, M., Dinkelborg, L., and Erdmann, V. A. (2004) *Nucleic Acids Res.* **19,** 5757–5765

18. Brandt, O., Feldner, J., Stephan, A., Schröder, M., Schnölzer, M., Arlinghaus, H. F., Hoheisel, J. D., and Jacob, A. (2003) *Nucleic Acids Res.* **31,** e119

19. Smith, D., Burgin, A. B., Haas, E. S., and Pace, N. R. (1992) *J. Biol. Chem.* **267,** 2429–2436

20. Sekiguchi, M., and Iida, S. (1967) *Proc. Natl. Acad. Sci. U. S. A.* **58,** 2316–2320

21. Hardt, W. D., Schlegl, J., Erdmann, V. A., and Hartmann, R. K. (1993) *Nucleic Acids Res.* **21,** 3521–3527

22. Dias, N., Sénamaud-Beaufort, C., le Forestier, E., Auvin, C., Hélène, C., and Saison-Behmoaras, T. E. (2002) *J. Mol. Biol.* **320,** 489–501

23. Geller, B. L., Deere, J. D., Stein, D. A., Kroeker, A. D., Moulton, H. M., and Iversen, P. L. (2003) *Antimicrob. Agents Chemother.* **47,** 3233–3239

24. Rebuffat, A. G., Nawrocki, A. R., Nielsen, P. E., Bernasconi, A. G., Bernal-Mendez, E., Frey, B. M., and Frey, F. J. (2002) *FASEB J.* **16,** 1426–1428

25. Vaara, M., and Porro, M. (1996) *Antimicrob. Agents Chemother.* **40,** 1801–1805; Correction (1997) *Antimicrob. Agents Chemother.* **41,** 496

26. Waugh, D. S., and Pace, N. R. (1990) *J. Bacteriol.* **172,** 6316–6321

27. Wegscheid, B., Condon, C., and Hartmann, R. K. (2006) *EMBO Rep.* **7,** 411–417

28. Brännvall, M., Pettersson, B. M. F., and Kirsebom, L. A. (2003) *J. Mol. Biol.* **325,** 697–709

29. Tackett, A. J., Corey, D. R., and Raney, K. D. (2002) *Nucleic Acids Res.* **4,** 950–957

30. Eckardt, S., Romby, P., and Sczakiel, G. (1997) *Biochemistry* **36,** 12711–12721

31. Kolb, F. A., Engdahl, H. M., Slagter-Jager, J. G., Ehresmann, B., Ehresmann, C., Westhof, E., Wagner, E. G., and Romby, P. (2000) *EMBO J.* **19,** 5905–5915

32. Nissen, P., Hansen, J., Ban, N., Moore, P. B., and Steitz, T. A. (2000) *Science* **289,** 920–930

33. Zasloff, M. (2002) *Nature* **415,** 389–395

34. Turner, J. J., Arzumanov, A. A., and Gait, M. J. (2005) *Nucleic Acids Res.* **1,** 27–42

35. Good, L., and Nielsen, P. E. (1998) *Proc. Natl. Acad. Sci. U. S. A.* **5,** 2073–2076